Pressure-induced cubic-to-orthorhombic phase transition in ZrW_2O_8

J. D. Jorgensen, Z. Hu, S. Teslic, D. N. Argyriou,* and S. Short
Materials Science Division, Argonne National Laboratory, Argonne, Illinois 60439

J. S. O. Evans†
Inorganic Chemistry, University of Oxford, South Parks Road, Oxford OX1 3QR, United Kingdom

A. W. Sleight
Department of Chemistry, Oregon State University, Corvallis, Oregon 97331

(Received 4 August 1998)

The crystal structure of ZrW_2O_8 and its variation with pressure and temperature have been investigated by *in situ* neutron powder diffraction. At room temperature, the cubic α phase is stable below 0.21 GPa, where a first-order transition to the orthorhombic γ phase, accompanied by a 4.95% reduction in volume occurs. The transition involves the inversion of one third of the W_2O_8 units, which is made possible by the migration of oxygen atoms that are bonded to only one W atom in the cubic phase. WO_4 tetrahedra tilt off the threefold axes of the cubic cell and oxygen atoms that are coordinated to only one W atom in the cubic phase become coordinated to two W atoms in the orthorhombic phase. In spite of its smaller volume, the orthorhombic phase has a volume compressibility $[(\Delta V/\Delta P)/V = -1.53(1)\times 10^{-2}\ \mathrm{GPa}^{-1}]$ that is slightly larger than that of the cubic phase $[-1.38(1)\times 10^{-2}\ \mathrm{GPa}^{-1}]$. This appears to result from a larger contribution of coordinated tilting of the ZrO_6 octahedra and WO_n polyhedra to the compression. The orthorhombic phase is retained upon release of pressure. Below room temperature, the metastable orthorhombic phase exhibits an average negative volume thermal expansion $[(\Delta V/\Delta T)/V]$ of $-3.4\times 10^{-6}\ \mathrm{K}^{-1}$, which is an order of magnitude smaller than that for the cubic phase $(-2.6\times 10^{-5}\ \mathrm{K}^{-1})$, apparently because of the reduced framework flexibility of the orthorhombic phase. Above room temperature, the thermal expansion of the orthorhombic phase becomes positive, prior to a first-order transition back to the cubic phase that occurs at about 390 K. [S0163-1829(99)01401-0]

INTRODUCTION

Zirconium tungstate, ZrW_2O_8, was recently shown to exhibit negative thermal expansion over the large temperature range 4 to 1050 K.[1] The compound remains cubic with isotropic contraction over the entire temperature range. ZrW_2O_8 and isostructural HfW_2O_8 are the only materials with isotropic negative thermal expansion over such a wide temperature range.[1,2] $Sc_2W_3O_{12}$ shows negative bulk thermal expansion over the temperature range 10–1200 K, but the thermal expansion is not isotropic.[3,4] It is negative along two of the three axes of the orthorhombic unit cell. Cubic ZrV_2O_7 shows isotropic negative thermal expansion only above 100 °C.[5,6] An anisotropic negative thermal expansion has been observed in other oxides, such as NZP,[7] but only above room temperature. The isotropic negative thermal expansion in cubic ZrV_2O_7 was attributed to the transverse vibration of the central oxygen atoms in the O_3V-O-VO_3 groups.[5] A similar mechanism was proposed to account for the thermal contraction in ZrW_2O_8.[1] The ZrW_2O_8 structure consists of ZrO_6 octahedra linked through oxygen atoms to WO_4 tetrahedra. Because of an unusually high degree of flexibility of the framework, rotational mode vibrations of the polyhedral units (called rigid unit modes), rather than bond-stretching vibrational modes, are thought to dominate the thermal expansion, even at low temperature. With increasing temperature, the structure contracts as the amplitudes of the rotational vibrations increase.[1,8,9]

A unique feature of the cubic ZrW_2O_8 structure [Fig. 1(a)] that contributes to this flexibility is the existence of an O atom associated with one of the two inequivalent WO_4 tetrahedra [O(4) in Fig. 2] that is bonded to only one W atom and is not bonded to any other metal atoms. The equivalent O atom in the other WO_4 tetrahedron [O(3)] is also bonded to only one W atom [W(2)], but interacts at a longer distance with the W atom in the neighboring tetrahedron [the W(1)-O(3) interaction in Fig. 2]. Within the two tetrahedra, the corresponding W-O bonds [W(2)-O(3) and W(1)-O(4) in Fig. 2] are aligned along the $\langle 111\rangle$ threefold axes of the cubic unit cell and point in the same direction for the nearest-neighbor WO_4 pairs [W(1)-W(2) group]. An order-disorder phase transition at 428 K from the acentric cubic α phase to the centric cubic β phase is associated with the mobility of the O(4) atom.[1,2] In the ordered α phase, the two tetrahedra associated with the W(1)-W(2) pair ''point'' in a specific direction. When the O(4) oxygen atom becomes mobile, it can bond with equal probability to either end of a W(1)-W(2) pair, giving equal probabilities for pointing in the $+[111]$ and $-[111]$ directions (and symmetry equivalent pairs). Thus, the disorder is made possible by the mobility of the one-coordinate O(4) atoms, which can detach themselves from the W atoms and move through the open framework structure to new sites. This degree of freedom, i.e., the inversion of a W_2O_8 unit made possible by oxygen atom migration, gives rise to the α-to-β order-disorder phase transition at 428 K. The inversion of a W_2O_8 unit is illustrated in

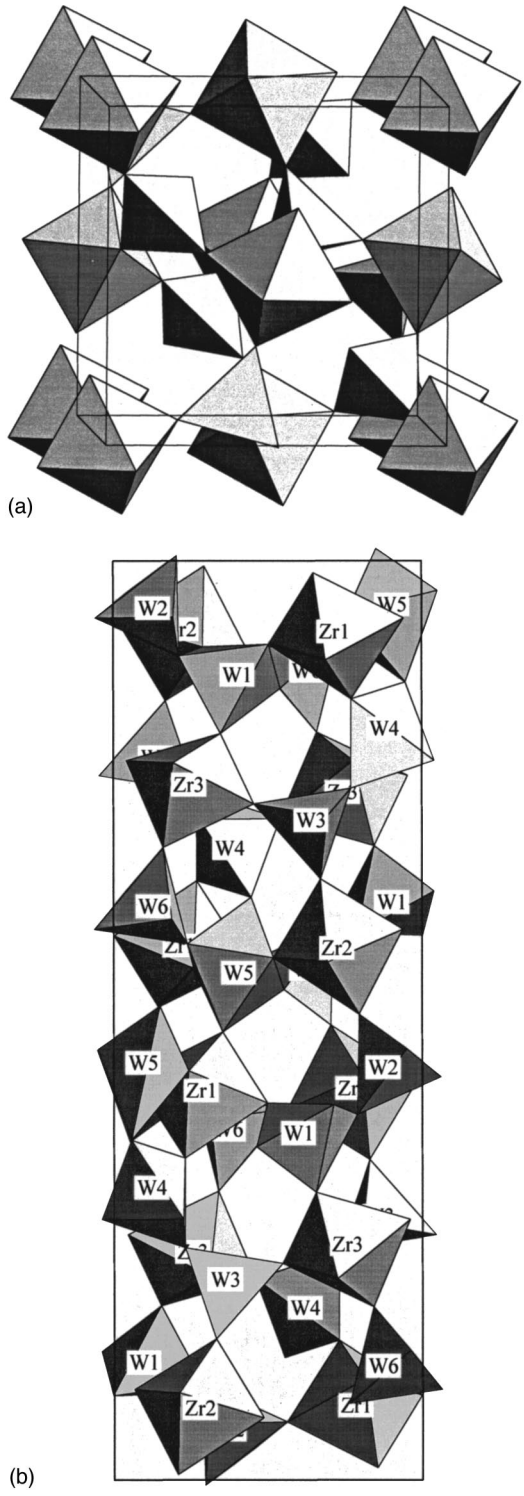

FIG. 1. Structures of the cubic α and orthorhombic γ phases of ZrW_2O_8 illustrated with ZrO_6 octahedra and WO_4 tetrahedra.

Fig. 3. In the disordered β phase, the orientations of the W_2O_8 units are random because the O(4) oxygen atoms are disordered. The W and O(3) sites also become disordered (but over a small distance) because the entire W(1)-W(2) pairs translate by a small amount along the $\langle 111 \rangle$ axes, with the oxygen atoms that link these tetrahedra to the ZrO_6 octahedra [O(1) and O(2) in Fig. 2] remaining essentially fixed in position, as the W(1)-W(2) pairs reverse directions.

The ZrW_2O_8 structural flexibility has been previously investigated by applying hydrostatic pressure. We have reported a pressure-induced phase transition from the cubic phase, α-ZrW_2O_8, to a complex orthorhombic structure, γ-ZrW_2O_8 (Fig. 1), accompanied by a 5% volume reduction.[10] The orthorhombic phase has a unit cell nominally three times larger than the cubic phase, as a result of inversion of one third of the W_2O_8 units. The orthorhombic phase is retained as a metastable phase after release of the pressure at room temperature, allowing its thermal-expansion properties to be compared to those of the cubic phase. The orthorhombic γ phase also shows negative volume thermal expansion from 20 to 300 K but an order of magnitude

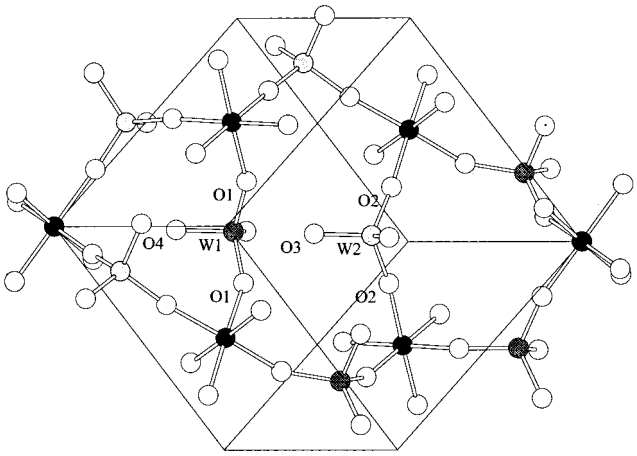

FIG. 2. A section of the cubic α phase ZrW_2O_8 structure viewed perpendicular to a threefold [111] axis with individual atoms shown. Atom labels are the same as in Table I.

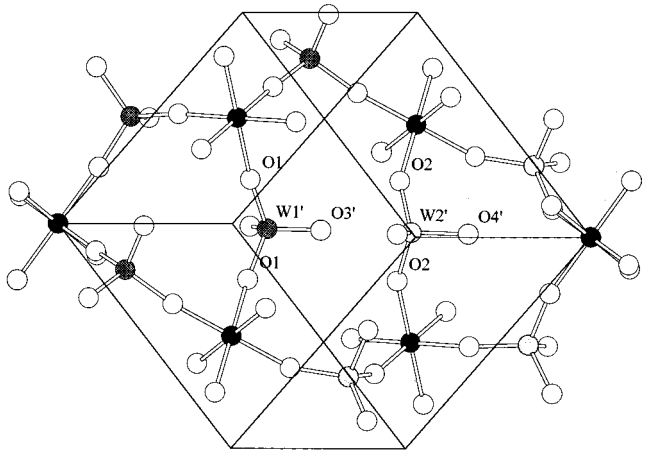

FIG. 3. Schematic illustration of what is meant by ''inversion'' of a W_2O_8 unit. The terminal oxygen atoms of the two WO_4 tetrahedra [O(3) and O(4) in Fig. 2] move from the original ''tip'' ends to the ''blunt'' ends. This requires migration of an O(4) atom, removing the original O(4) atom (Fig. 2) and placing a new atom at O(4′), and a very small displacement of the O(3) atom to a new position, O(3′), bonded to the other W atom. There is a small translation of the two W atoms along the [111] axis because the oxygen atoms [O(1) and O(2)] that link the WO_4 tetrahedra to the ZrO_6 octahedra remain in nominally the same positions. The new O(4′) atom is likely to come from the tip of a nearby W_2O_8 group (requiring a migration path of only 4.2 Å) not from the same W_2O_8 group.

smaller than that for the α or β phases. The metastable orthorhombic γ phase can be transformed back to the cubic α phase by heating above 390 K at ambient pressure. This paper presents a full description of the pressure-induced phase transition, the compression of both the orthorhombic and cubic phases, the thermal-expansion properties of the orthorhombic phase, and the transition back to the cubic phase upon heating.

SAMPLE PREPARATION

The measurements described here were made on two different samples. A 6 g sample was made at Oregon State University. Reactants were appropriate quantities of $ZrOCl_2 \cdot 8H_2O$ and H_2WO_4. The $ZrOCl_2 \cdot 8H_2O$ was dissolved in water. The H_2WO_4 was dissolved in aqueous NH_4OH. The tungstate solution was brought to boiling and its pH adjusted to 5 by addition of aqueous HCl. The Zr^{4+} containing solution was added to the hot solution containing W^{6+}. This mixture was evaporated to dryness on a hot plate. The solid product was ground and heated at 600 °C for 2 h. This product was cooled to room temperature, ground, heated at 1200 °C for 1 h, and cooled by removing the sample from the furnace. This sample was used for the initial measurements.[10] To allow faster neutron-diffraction measurements (including inelastic neutron-scattering measurements, to be reported separately), a larger sample ($\sim$100 g) was later obtained from Wah Chang. The synthesis method used by Wah Chang was the same. However, they used larger amounts, which inevitably leads to a somewhat slower cooling rate and, therefore, slight decomposition. These two samples showed essentially identical lattice parameters and were assumed to be the same except that the sample from Wah Chang contains traces of ZrO_2 and WO_3 impurities (visible by x-ray diffraction, but not prominent in neutron-diffraction patterns), which give it a light yellowish color. These impurities are thought to result from decomposition that occurs during cooling between about 1200 and 800 °C because of the slower cooling rate. In the later stages of our experiments we observed a subtle difference in the pressure-induced phase transitions for the two samples. This is discussed in the following section.

NEUTRON DIFFRACTION MEASUREMENTS

Neutron-diffraction data were collected as a function of pressure at room temperature and as a function of temperature at ambient pressure. The experiments were performed at the Argonne National Laboratory using the Special Environment Powder Diffractometer (SEPD) at the Intense Pulsed Neutron Source.[11] For high-pressure measurements the samples were contained in a thin walled vanadium tube which was inserted into a helium gas pressure cell.[12] Using helium gas as the pressure medium, the pressure cell provides hydrostatic pressure to 0.65 GPa over the temperature range of 40–300 K, with the ability to vary pressure and temperature *in situ*. The collimation of the cell and the diffraction geometry ensure that the diffraction data are free of Bragg scattering from the cell. For low- and high-temperature measurements at ambient pressure the samples were contained in sealed vanadium cans with helium exchange gas. The low-temperature (20–300 K) data were collected using a displex refrigerator while the high-temperature data (300–473 K) were collected using a simple radiation furnace. 300 K data at ambient pressure were recorded in the pressure cell, displex refrigerator, and furnace to provide a method for correcting for small errors in the measurement of lattice parameters that can result from differences in sample positioning.

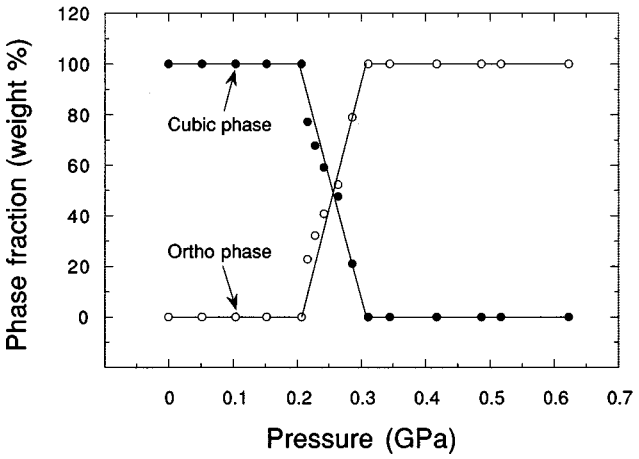

FIG. 4. Fractions of the cubic and orthorhombic phases vs pressure based on the results of two-phase Rietveld refinements. Data taken with the Wah Chang sample upon increasing pressure (see text).

Three separate experiments were done at room temperature as a function of pressure. In the first experiment, the sample from Oregon State University was studied at 0 GPa (for 6 h), 0.21 GPa (8 h), 0.42 GPa (10 h), and 0.62 GPa (8 h) upon increasing pressure and 0.52 GPa (7 h), 0.31 GPa (7 h), 0.10 GPa (8 h) upon decreasing pressure. The sample was a mixture of orthorhombic and cubic phases at 0.21 GPa and fully orthorhombic at 0.42 GPa and remained orthorhombic after release of pressure. The larger sample from Wah Chang was then used to achieve a faster counting rate, enabling measurements at closely spaced pressures, in an attempt to fully characterize the pressure induced phase transition and establish an accurate transition pressure. Data were collected at pressures of 0 GPa (4 h), 0.05 GPa (4 h), 0.11 GPa (4 h), 0.16 GPa (4 h), 0.21 GPa (3 h), 0.22 GPa (2 h), 0.24 GPa (1 h), 0.25 GPa (1 h), 0.27 GPa (3 h), 0.30 GPa (2 h), 0.32 GPa (4 h), 0.36 GPa (4 h), and 0.50 GPa (4 h) upon increasing pressure. Beginning at 0.21 GPa, a mixed-phase region with an increasing fraction of the orthorhombic phase upon continuing to increase pressure was observed. The transition was complete at 0.32 GPa. Figure 4 shows the fractions of the cubic and orthorhombic phases vs pressure based on the results of two-phase Rietveld refinements (which will be described later). In a third measurement using the sample from Oregon State University, the sample was pressurized to 0.22 GPa and data were collected in sequential runs of 1 h each at constant pressure. The transformation to the orthorhombic phase occurred over a period of time and was complete in 6 h. Thus, the Oregon State University and Wah Chang samples differ in a subtle way in the kinetics and pressure dependence of the cubic-to-orthorhombic phase transition. The transition begins at 0.21 GPa for both samples, within

the precision of our measurements. The Oregon State University sample transforms fully at constant pressure over a period of 6 h, while the Wah Chang sample requires a further increase of pressure to 0.32 GPa to produce a full transformation. The transformation kinetics for the Wah Chang sample were not investigated in a separate measurement, but it is clear that it would not have transformed at constant pressure over a period of 12 h because of the time required for the transformation even with the application of increasing pressure. This behavior suggests that the phase transition may be very sensitive to small variations in chemical composition (not apparent in other measurements) or to differences in the grain size and sintering between grains. Grain-interaction stresses could modify the pressure seen by individual grains even though the helium pressure medium is perfectly hydrostatic. These subtle differences were not investigated further.

Neutron-diffraction data from the Oregon State University sample after removal from the pressure cell were collected as a function of increasing temperature at temperatures of 348, 373, 391, 398, 423, and 473 K. The orthorhombic phase was retained until about 373 K, but the sample transformed back to the cubic α phase with no measurable transition kinetics at 391 K.

DATA ANALYSIS

The neutron powder-diffraction data were analyzed by the Rietveld method using the GSAS program.[13] In high-pressure measurements only the 90° data ($\Delta d/d = 0.05$) were collected and analyzed. The backscattering, 145°, high-resolution data ($\Delta d/d = 0.035$) were analyzed for ambient-pressure measurements done outside the pressure cell. The 90° data were refined over a *d*-spacing range of 1–4.65 Å which included 175 peaks for the cubic and/or 1304 peaks for the orthorhombic phase. For the 145° data the *d*-spacing range was 1–3.95 Å and included 172 peaks for the cubic and/or 1286 peaks for the orthorhombic phase. The data in the cubic phase were analyzed with the same model (space group $P2_13$) as used by Mary *et al.*[1] Refined structural parameters in the cubic phase were the fractional atomic coordinates, cell parameters, profile parameters, background terms, and anisotropic temperature factors for all atoms (54 parameters total). The orthorhombic model (space group $P2_12_12_1$) has been presented previously.[10] This is a challenging structure to refine using the 90° data from the high-pressure cell because of the large number of parameters for the 33 inequivalent atoms in the cell. For this reason, only three temperature factors (one for each chemical species) were refined, giving 136 parameters total. In the mixed-phase region, the refined scale factors provided a measure of the relative phase fractions (Fig. 4).

The observed, calculated, and difference profiles from Rietveld refinements for the room-temperature data (the Wah Chang sample) at three pressures are shown in Fig. 5. Pattern (a) corresponds to cubic ZrW_2O_8 at ambient pressure; pattern (b) represents a 48% cubic, 52% orthorhombic ZrW_2O_8 mixture (in weight percentages) at 0.26 GPa; and pattern (c) is for the fully converted orthorhombic ZrW_2O_8 at 0.62 GPa. The signal-to-background ratios and scale factors were as expected for all measurements, leading to the conclusion that no significant amounts of amorphous or highly disordered material were present at any pressure. A Rietveld refinement plot for the orthorhombic phase at ambient pressure and 20 K, at the higher resolution provided by the 145° scattering angle, is also shown in Fig. 5(d). Tables I and II give refined structural parameters for the cubic and metastable orthorhombic structures at room temperature and ambient pressure, where the higher resolution back-scattering data could be refined.

RESULTS AND DISCUSSION

The unit-cell volumes vs pressure for the cubic α phase and orthorhombic γ phase at room temperature are shown in Fig. 6. The volume compressibility of the cubic phase, defined as $(\Delta V/\Delta P)/V$, is $-1.38(1)\times10^{-2}$ GPa^{-1}. The volume compressibility of the orthorhombic phase is $-1.53(1)\times10^{-2}$ GPa^{-1}. The slightly larger compressibility for the orthorhombic phase, in spite of its smaller cell volume, suggests that the compression mechanisms could be different.

Identifying the compression mechanism that is operative in the α phase is difficult because the α phase exists only over a small pressure range (0–0.2 GPa). Thus, even though the diffraction data are of high quality, the pressure dependence of bond lengths and angles can be determined only with a limited precision. Various bond lengths and angles vs pressure are shown in Fig. 7. It is common in covalently bonded compounds that consist of corner sharing polyhedra that compression occurs by a coordinated tilting of polyhedra which brings them closer together. Therefore, we investigated the Zr-O(1)-W(1) and Zr-O(2)-W(2) bond angles, which characterize relative tilting of ZrO_6 and WO_4 polyhedra (Fig. 2). Both angles increase with increasing pressure [Fig. 7(a)]. Intuitively, one would expect that increases of these angles would lead to expansion, not compression. However, a distance-least-squares refinement[14] for an idealized cubic ZrW_2O_8 structure (with perfect, rigid polyhedra) as a function of changing the unit-cell volume gives the surprising result that, over a limited range of cell volumes (volumes that correspond to negative pressure in the model calculation), compression can occur by *increasing* the average Zr-O-W angle. This model calculation suggests that the unusual bonding present in α-ZrW_2O_8 may lead to a situation where the normal relationship between cell volume and polyhedral linking angles does not occur. This could explain the unexpected increase of Zr-O-W angles with pressure.

The data also suggest a shortening of the Zr-O distances with increasing pressure [Fig. 7(b)], implying a compression of the ZrO_6 octahedra. However, this effect is just outside the experimental error. Moreover, based on observations of compression in other framework structures involving ZrO_6 octahedra, one would not expect a significant compression of Zr-O bonds.[15] Additional data with higher precision would be required to confirm whether significant Zr-O bond compression occurs in α-ZrW_2O_8.

The W-O distances do not change significantly. However, there is evidence for pressure-induced distortion of the WO_4 tetrahedra. In the cubic α phase, the tetrahedron surrounding W(1) is compressed along the threefold axis, taking the shape of a trigonal pyramid (Figs. 2). The angles between the

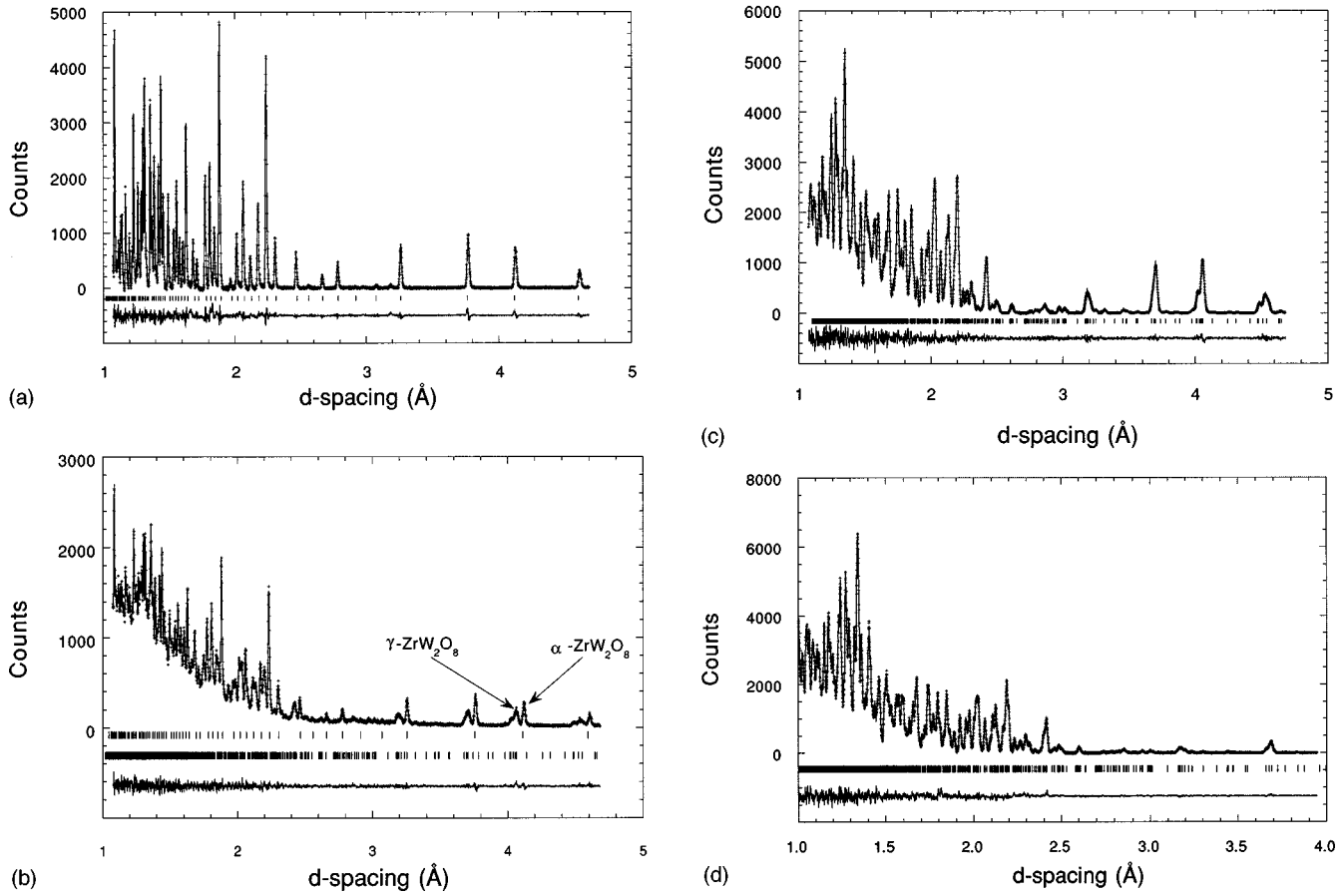

FIG. 5. Time-of-flight neutron-diffraction patterns for (a) cubic α-ZrW_2O_8 at 300 K and atmospheric pressure, (b) 48% α-ZrW_2O_8, 52% γ-ZrW_2O_8 at 0.26 GPa, (c) fully converted orthorhombic γ-ZrW_2O_8 at 0.62 GPa and (d) orthorhombic γ-ZrW_2O_8 at 20 K and ambient pressure with the higher resolution provided by the backscattering detector banks. The observed (+), calculated (solid line), and difference (lower solid trace) profiles from the Rietveld refinements are shown. Tick marks below the profile indicate the positions of allowed Bragg reflections. Background has been subtracted prior to plotting for all patterns.

three basal oxygen atoms [O(1)], W(1), and the apical oxygen atom [O(4)] are inequivalent by symmetry to the angles between pairs of the three basal oxygen atoms [O(1)] and W(1) (Figs. 2). At the ambient pressure, the O(1)-W(1)-O(4) and O(1)-W(1)-O(1) angles are 101.7° and 115.9°, respectively, compared with a value of 109.5° for an ideal tetrahedron. The W(2) tetrahedron is almost perfect with O(2)-W(2)-O(2) and O(2)-W(2)-O(3) angles of 109.7° and 109.0°, respectively. Strong inter-tetrahedral O(1)-O(3) repulsion may explain the observed deformation of the W(1) tetrahedron and lack of deformation for the W(2) tetrahedron. With increasing pressure, the W(1) atom gets even closer to the tetrahedral face perpendicular to the threefold axis resulting in increased distortion due to a decrease of the O(1)-W(1)-O(4) angle and an increase of the O(1)-W(1)-O(1) angle [Fig. 7(c)]. Applied pressure has an opposite effect on the W(2) tetrahedral angles—increase of the O(2)-W(2)-O(3) angle and decrease of the O(2)-W(2)-O(2) angle [Fig. 7(c)], but the distortion remains small for this tetrahedron. However, the W(2) atom moves away from the W(2)O(2) tetrahedral face perpendicular to the threefold axis and gets closer to the W(1) atom. From 0 to 0.21 GPa, the compressibility of

TABLE I. Refined structural parameters for cubic α-ZrW_2O_8 at room temperature and ambient pressure. Numbers in parentheses are standard deviations from Rietveld refinement. Space group $P2_13$, $a=9.1494(1)$ Å, $wR_p=0.0642$, $R_p=0.0956$, $R(F^2)=0.0712$, $\chi^2=2.035$.

Atom	x	y	z	U11	U22	U33	U12	U13	U23
Zr	0.0011(3)	0.0011(3)	0.0011(3)	0.0042(5)	0.0042(5)	0.0042(5)	0.0013(8)	0.0013(8)	0.0013(8)
W(1)	0.3401(3)	0.3401(3)	0.3401(3)	0.0071(14)	0.0071(14)	0.0071(14)	0.0051(15)	0.0051(15)	0.0051(15)
W(2)	0.6006(3)	0.6006(3)	0.6006(3)	0.0050(13)	0.0050(13)	0.0050(13)	0.0008(12)	0.0008(12)	0.0008(12)
O(1)	0.2055(4)	0.4376(4)	0.4467(4)	0.0091(20)	0.0163(26)	0.0228(25)	0.0074(17)	0.0094(18)	−0.0030(18)
O(2)	0.7877(3)	0.5694(4)	0.5549(4)	0.0012(19)	0.0198(23)	0.0181(24)	0.0074(16)	0.0026(19)	0.0054(16)
O(3)	0.4922(5)	0.4922(5)	0.4922(5)	0.0178(10)	0.0178(10)	0.0178(10)	−0.0083(14)	−0.0083(14)	−0.0083(14)
O(4)	0.2323(3)	0.2323(3)	0.2323(3)	0.0290(15)	0.0290(15)	0.0290(15)	−0.0114(15)	−0.0114(15)	−0.0114(15)

TABLE II. Refined structural parameters for metastable orthorhombic γ-ZrW_2O_8 at room temperature and ambient pressure. Numbers in parentheses are standard deviations from Rietveld refinement. Space group $P2_12_12_1$, $a=9.0608(2)$ Å, $b=27.0141(6)$ Å, $c=8.9191(2)$ Å, $wR_p=0.0382$, $R_p=0.0251$, $R(F^2)=0.0292$, $\chi^2=1.715$.

Atom	x	y	z	U
Zr(1)	0.2117(8)	0.4215(3)	0.8074(9)	0.0007(18)
Zr(2)	0.7238(9)	0.4243(3)	0.2291(9)	0.0007(18)
Zr(3)	0.7439(10)	0.2549(4)	0.7410(10)	0.0007(18)
W(1)	0.9025(17)	0.3730(5)	0.5787(16)	0.0001(14)
W(2)	0.6319(13)	0.4488(5)	0.8306(16)	0.0001(14)
W(3)	0.1497(16)	0.2186(6)	0.8587(14)	0.0001(14)
W(4)	0.3788(15)	0.3169(6)	0.6132(16)	0.0001(14)
W(5)	0.4033(14)	0.4498(6)	0.4627(15)	0.0001(14)
W(6)	0.1236(14)	0.3789(6)	0.2114(15)	0.0001(14)
O(11)	0.7128(14)	0.5924(4)	0.9595(12)	0.0066(9)
O(12)	0.6508(13)	0.6862(5)	0.1428(12)	0.0066(9)
O(13)	0.4991(12)	0.5926(4)	0.2327(12)	0.0066(9)
O(101)	0.4554(12)	0.6390(4)	0.9526(11)	0.0066(9)
O(21)	0.6887(12)	0.4416(5)	0.0211(12)	0.0066(9)
O(22)	0.4361(12)	0.4394(4)	0.8527(13)	0.0066(9)
O(23)	0.7082(13)	0.5057(4)	0.7801(12)	0.0066(9)
O(102)	0.7897(12)	0.6030(4)	0.2444(12)	0.0066(9)
O(31)	0.6685(12)	0.3469(4)	0.1963(13)	0.0066(9)
O(32)	0.6898(13)	0.2771(4)	0.9434(13)	0.0066(9)
O(33)	0.4478(13)	0.2674(5)	0.1726(12)	0.0066(9)
O(103)	0.4441(10)	0.3669(4)	0.5072(13)	0.0066(9)
O(41)	0.2273(12)	0.6494(4)	0.2540(12)	0.0066(9)
O(42)	0.9572(14)	0.7151(5)	0.1682(12)	0.0066(9)
O(43)	0.2165(13)	0.7204(4)	0.9688(12)	0.0066(9)
O(104)	0.7642(12)	0.2502(5)	0.2508(12)	0.0066(9)
O(51)	0.3563(14)	0.5133(5)	0.3963(14)	0.0066(9)
O(52)	0.9786(14)	0.5671(4)	0.7974(12)	0.0066(9)
O(53)	0.2352(14)	0.5566(4)	0.1041(12)	0.0066(9)
O(105)	0.9540(12)	0.5383(4)	0.0883(14)	0.0066(9)
O(61)	0.1846(14)	0.3943(5)	0.0288(11)	0.0066(9)
O(62)	0.1595(13)	0.3155(4)	0.2128(12)	0.0066(9)
O(63)	0.9418(15)	0.4031(5)	0.1892(14)	0.0066(9)
O(106)	0.2570(14)	0.5817(4)	0.8152(10)	0.0066(9)

the W(1)-W(2) distance $[\Delta l//\Delta P)l]$ is -1.8×10^{-2} GPa^{-1} [Fig. 7(d)], which is substantially larger than the linear unit-cell compressibility, $(\Delta a/\Delta P)/a=-4.69\times10^{-3}$ GPa^{-1}. Most of the decrease in the W(1)-W(2) distance comes from a large compressibility $[\Delta l//\Delta P)/l]$ of the W(1)-O(3) distance $[-7.0\times10^{-2}$ GPa^{-1}, Fig. 7(d)].

The result of these changes in bond lengths and angles, and distortions of the polyhedra, is that the Zr-W distances decrease as shown in Fig. 7(e). Because of the unusual bonding of the cubic structure, the shorter Zr-W distance, Zr-W(1), has a compressibility $(-7.2\times10^{-3}$ $GPa^{-1})$ about twice that of the linear compressibility of the unit cell $(-4.69\times10^{-3}$ $GPa^{-1})$, while the Zr-W(2) distance is almost constant with pressure $(-1\times10^{-4}$ $GPa^{-1})$.

The pressure-induced transition from the cubic α phase to the orthorhombic γ phase is most easily understood in terms of an ''inversion'' of one third of the W_2O_8 units. In the cubic α phase, pairs of W atoms lie along the $\langle111\rangle$ threefold axes of the cubic unit cell [the W(1)-W(2) pair illustrated in Fig. 2]. The oxygen atoms bonded to these W atoms form two WO_4 tetrahedra pointed in a specific direction. When the cubic α phase transforms to the orthorhombic γ phase, terminal oxygen atoms are rearranged such that one third of these W_2O_8 units (those involving W(3) and W(4) in the orthorhombic phase) reverse their direction. This inversion of one third of the W_2O_8 units results in a tripling of the unit-cell volume to form the new orthorhombic cell. The inversion of a W_2O_8 unit is illustrated schematically in Fig. 3. The inversion requires the coordinated diffusion of a terminal O(4) oxygen atom (Fig. 2) over a distance of about 4.2 Å from the ''tip'' of one W_2O_8 unit to the ''blunt end'' of another unit, while the original ''tip'' oxygen atom of the neighboring W_2O_8 unit diffuses to the ''blunt end'' of a fourth unit, and so on throughout the structure. In the α-to-γ transition, when one third of the W_2O_8 units invert, the remaining structure relaxes. In particular all of the WO_4 tetrahedra tilt off the original threefold axes in such a way that their terminal oxygen atoms become associated with neighboring W atoms.

There is a 4.95(3)% volume reduction at the cubic-to-orthorhombic phase transition as determined from refinements in the mixed-phase pressure range for the Wah Chang sample. This volume reduction appears to result from the topological changes in the W-O sublattice—specifically, from the additional W-O bonding that is made possible by the inversion and the resulting tilts of WO_n polyhedra. The threefold symmetry present in the cubic phase is broken in the orthorhombic structure by tilting of the WO_4 tetrahedra off the $\langle111\rangle$ axes, as shown in Fig. 8. There are three inequivalent Zr atoms (ZrO_6 octahedra) and six inequivalent W atoms (WO_n polyhedra) in the orthorhombic phase instead of one and two, respectively, in the cubic α phase. The tetrahedral tilting allows the oxygen atom [O(4) in Fig. 2] that was previously coordinated to only one W atom to become coordinated to a second W atom. Thus, all oxygen atoms are two-coordinated in the orthorhombic phase. The oxygen valence, calculated using bond valence sum techniques,[16] changes significantly. The valence of the originally one-coordinate oxygen atom [O(4)] changes from 1.72

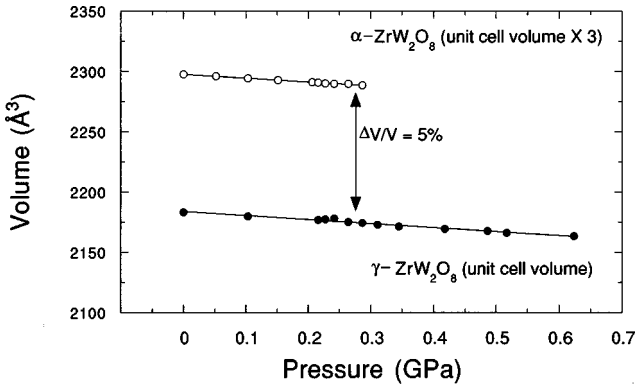

FIG. 6. Unit-cell volumes of the cubic α-ZrW_2O_8 and orthorhombic γ-ZrW_2O_8 phases vs applied pressure. Solid lines are linear least-squares fits to the data. Because the orthorhombic phase, is retained upon release of pressure after being formed, its properties can be measured over the full pressure range.

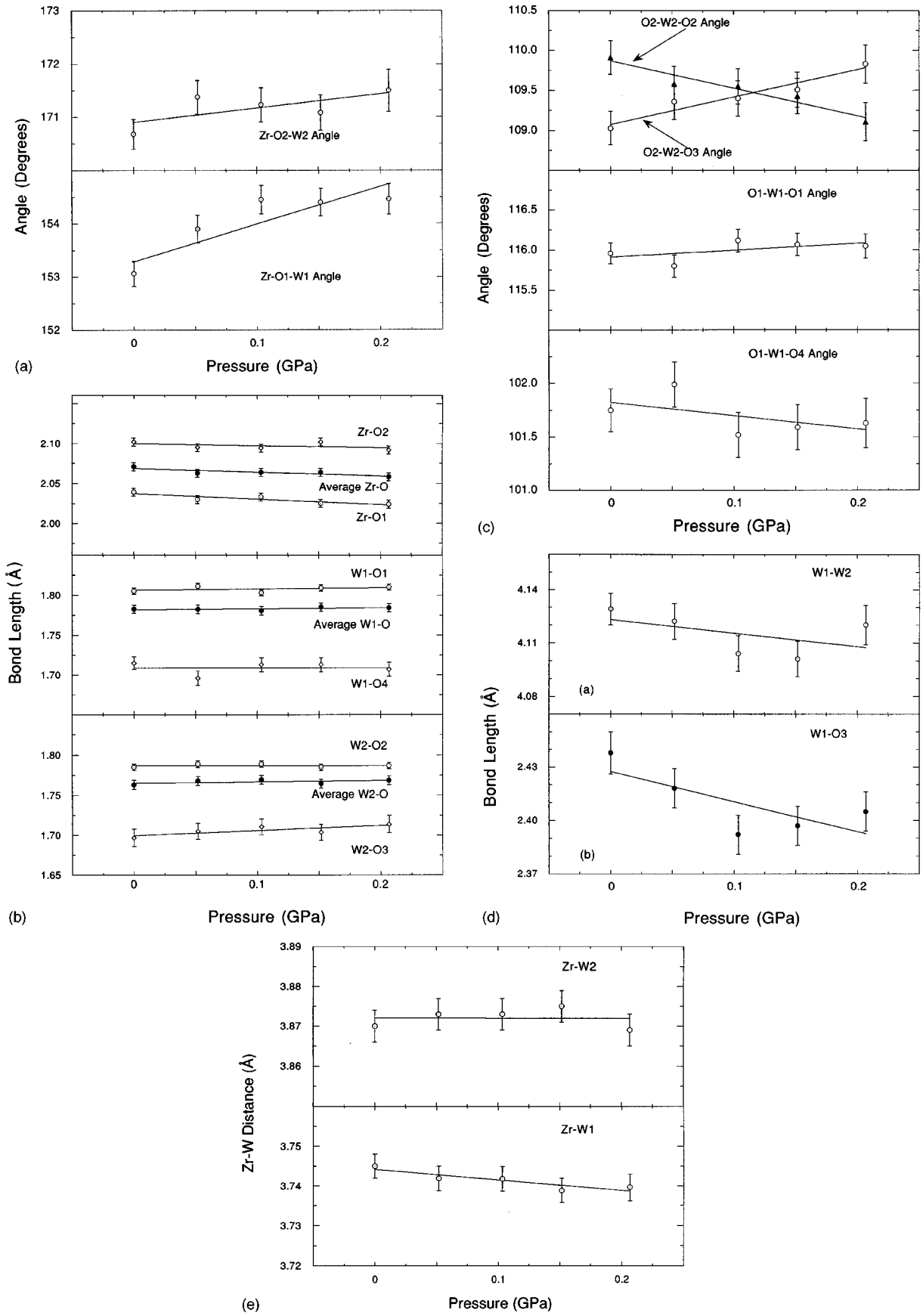

FIG. 7. (a) Zr-O-W bond angles, (b) W-O bond lengths, (c) O-W-O bond angles, (d) W(1)-W(2) interatomic distance and W(1)-O(3) bond length, and (e) Zr-W distances in cubic α-ZrW_2O_8 over the pressure range of 0–0.21 GPa. Solid lines are linear least-squares fits to the data.

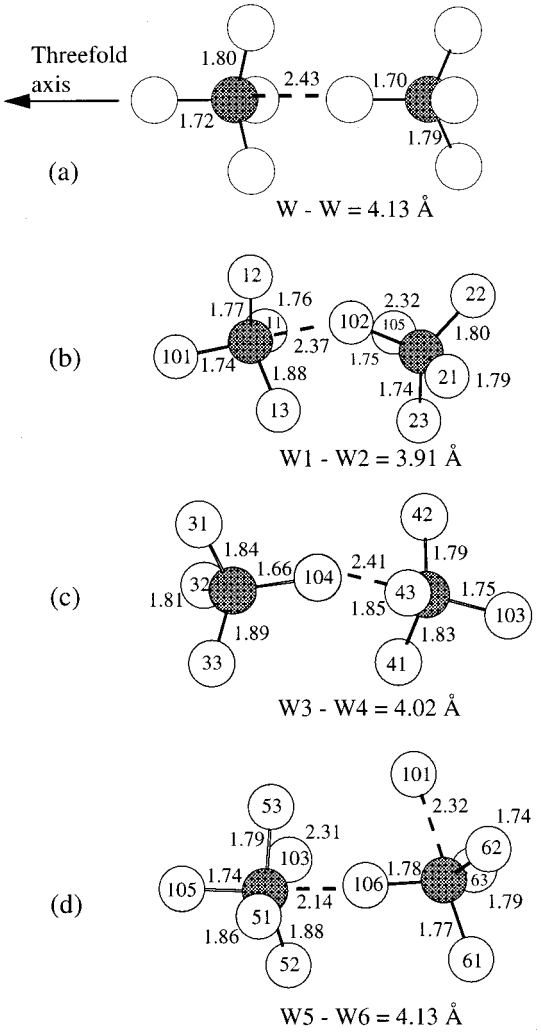

FIG. 8. Structural arrangement of the WO_4 groups of (a) cubic α-ZrW_2O_8 and (b, c, and d) orthorhombic γ-ZrW_2O_8 phase, viewed perpendicular to a threefold $\langle 111 \rangle$ axis in the cubic α phase. Bond lengths are shown in angstroms. Open symbols are oxygen atoms; W atoms are shaded. Bond distances less than 2.3 Å are drawn as solid lines; longer distances, as dashed lines. Atom labels are the same as in Tables I and II.

to 1.96 (average of the three corresponding oxygen atoms in the orthorhombic structure), while the valence of the O(3) atom changes only slightly from 2.07 to 2.06. Thus, in the orthorhombic phase, all oxygen atoms attain a calculated valence near 2. Additionally, whereas the WO_n polyhedra can be viewed as tetrahedra with four oxygen atoms bonded to each W atom in the cubic phase, this is not the case in the orthorhombic phase, where the bonding of oxygen atoms to the W atoms is more complex and is significantly different for each W atom (as shown in Fig. 8).

The best comparison of the cubic and orthorhombic structures comes from refinements using data taken at ambient pressure outside the pressure cell, where the high-resolution back-scattering data can be used (see Tables I and II). Comparisons of bond lengths and angles for the cubic and orthorhombic phases are done using these data. The degree of polyhedral tilting in the γ phase is characterized by the Zr-O-W angles. Each of the two Zr-O-W angles in the cubic phase corresponds to nine Zr-W-O angles in the orthorhombic phase. The Zr-O-W(1) angle in the cubic phase (153.0°) is significantly larger than the average of the γ-phase Zr-O-W angles which correspond to it (145.9°). Similarly, the α-phase Zr-O-W(2) angle (170.7°) is larger than average of the corresponding γ-phase Zr-O-W angles (168°). In spite of this reduction in Zr-O-W angles, the Zr and W atoms do not move significantly closer. The average Zr-W distance is 3.808(2) Å in the cubic phase and 3.799(3) Å in the orthorhombic phase (only 0.2% shorter). This leads to the conclusion that the compression must come from the changes in the W-O bonding. Because of the inversion of one third of the W_2O_8 groups, these changes cannot be viewed in a simple way; i.e., it is not possible to correlate all bonds and angles in the orthorhombic structure to their counterparts in the cubic structure. However, some general observations can be made. The W(1)-W(2) distance within a pair of tetrahedra in the cubic structure is 4.129(9) Å. In the orthorhombic structure, the three corresponding distances are $d[\mathrm{W(1)\text{-}W(2)}] = 3.905(20)$ Å, $d[\mathrm{W(3)\text{-}W(4)}] = 4.018(23)$ Å, and $d[\mathrm{W(5)\text{-}W(6)}] = 3.891(18)$ Å, giving an average of 3.968(12) Å (4% shorter). Changes in other W-W distances are more difficult to evaluate. In the cubic structure, each W(1) atom has three W(2) second nearest neighbors at a distance of 4.621(4) Å, and vice versa. In the orthorhombic structure, the number of second-nearest-neighbor W atoms at a distance of less than 5 Å is different for every W atom: four for W(1), three for W(2), two for W(3), seven for W(4), three for W(5), and three for W(6). The most remarkable changes are for the W(3)-W(4) pair that is inverted. Because the W-W arrangement is so different in the orthorhombic structure, it is not meaningful to compare W-W bond distances. However, the data suggest that the changes in the W-O bonding and the resulting compression of the W-O sublattice is principally responsible for the 5% volume reduction.

A striking feature of the γ-ZrW_2O_8 structure is the lack of similarity among the symmetry-independent polyhedral units (Fig. 8). Most W atoms become five-coordinated with one long W-O distance and their oxygen environments take the shape of distorted trigonal bipyramids (Fig. 8). Only the oxygen atoms around W(3) form an almost perfect tetrahedron with an average (apical O)-W(3)-(basal O) angle of 110.0° and (basal O)-W(3)-(basal O) angle of 108.8°. The other five symmetry inequivalent polyhedra are highly deformed. For example, the average (apical O)-W(1)-(basal O) angle is 98.3° in contrast to the average (basal O)-W(1)-(basal O) angle which is 117.8°. The respective angles in the W(2) polyhedron are 109.2° and 118.8°, in the W(4) polyhedron 102.7° and 115.2°, and in the W(6) polyhedron 97.4° and 118.4°.

The compression mechanism in the orthorhombic phase is difficult to describe owing to the large number of atoms in the unit cell. An informative qualitative view of the compression can be based on the observed pressure dependence of average bond lengths and angles. Such an approach leads to the conclusion that coordinated tilting of the polyhedra, as is typical for covalently bonded framework solids, is an important contribution to the compression in the orthorhombic phase. The average Zr-O-W bond angle decreases significantly with pressure, as shown in Fig. 9(a). The average

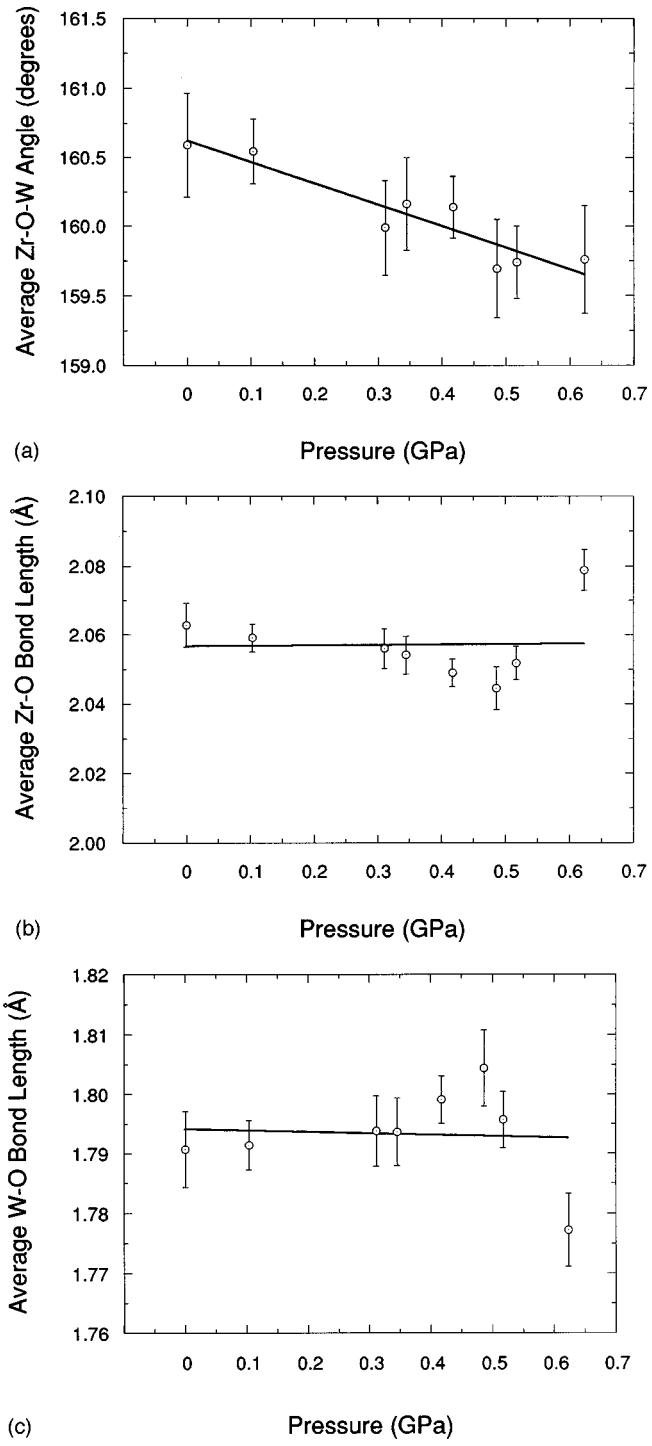

FIG. 9. (a) Average Zr-O-W bond angle, (b) Zr-O bond length, and (c) W-O bond length vs pressure for orthorhombic γ-ZrW_2O_8. Solid lines in (a), (b), and (c) are linear least-squares fits to the data.

Zr-O and W-O bond lengths are nominally constant, as shown in Figs. 9(b) and 9(c). Because so many inequivalent angles and distances are involved, it is not possible to describe distortion of individual polyhedra vs pressure. The increased contribution of coordinated tilting is probably responsible for the slightly higher volume compressibility for the orthorhombic phase [$-1.53(1)\times10^{-2}$ GPa^{-1} vs $-1.38(1)\times10^{-2}$ GPa^{-1} for the cubic phase], even though its volume is 5% smaller. Apparently, the lowering of symmetry and tilting of the WO_4 tetrahedra off the threefold axes

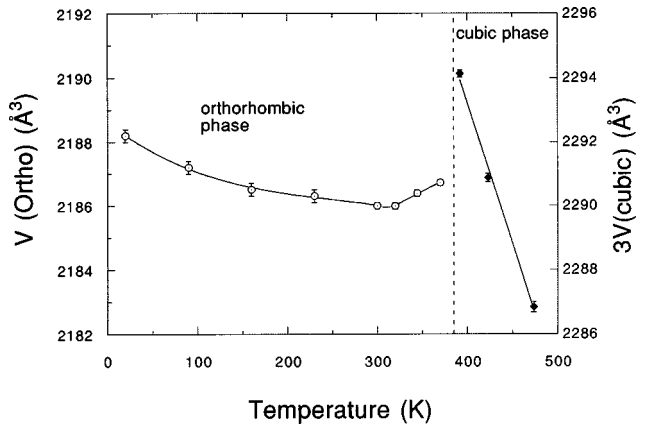

FIG. 10. Unit-cell volume of orthorhombic γ-ZrW_2O_8 and cubic α-ZrW_2O_8 vs temperature over a temperature range of 20–473 K. Data were obtained by heating the metastable orthorhombic phase through the transition back to the cubic phase.

allows this tilting mechanism of compression to occur in the orthorhombic phase, whereas symmetry and bonding constraints prevent it in the cubic phase.

In our previous neutron powder-diffraction study[10] we measured the temperature dependence of the γ-ZrW_2O_8 unit-cell parameters and volume over a range of 20 to 300 K. We found that γ-ZrW_2O_8 has an average negative volume coefficient of thermal expansion of -3.4×10^{-6} K^{-1} in the temperature range of 20–300 K, which is an order of magnitude smaller than that for α- or β-ZrW_2O_8 (-2.6×10^{-5} K^{-1}, averaged over the temperature range of 4–693 K). In the present work we collected data at more temperatures and over a wider temperature range, 20–473 K. Figure 10 shows the γ-ZrW_2O_8 cell volume for the Oregon State University sample over this temperature range. As observed previously, the γ phase has a negative thermal expansion below room temperature. However, the magnitude of the coefficient of thermal expansion decreases gradually and becomes zero around room temperature. Above room temperature, as the transition to the cubic α phase is approached, the cell volume increases. There is a first-order transition to the cubic phase between 373 and 391 K. Above the phase transition, the volume coefficient of thermal expansion is again negative. The increase in unit-cell volume at the phase transition is about 5%, which corresponds in magnitude to the volume change induced by pressure in the cubic-to-orthorhombic phase transition. Using neutron diffraction, data were not taken at enough closely spaced temperatures to investigate mixed phase (i.e., cubic plus orthorhombic) behavior at this transition. However, separate laboratory x-ray measurements suggest that a mixed-phase region perhaps 15° wide may exist at temperatures of 380–395 K. Such effects could depend on subtle properties of the sample being studied (as we observed for the pressure-induced transition) and were not investigated further.

The temperature dependences of the lattice parameters of the orthorhombic γ phase as the transition to the cubic α phase is approached are shown in Fig. 11. Below room temperature, all lattice parameters show a small decrease with increasing temperature. Above room temperature, the lattice parameters behave rather differently; while *a* and *b* increase with temperature approaching the phase transition, *c* de-

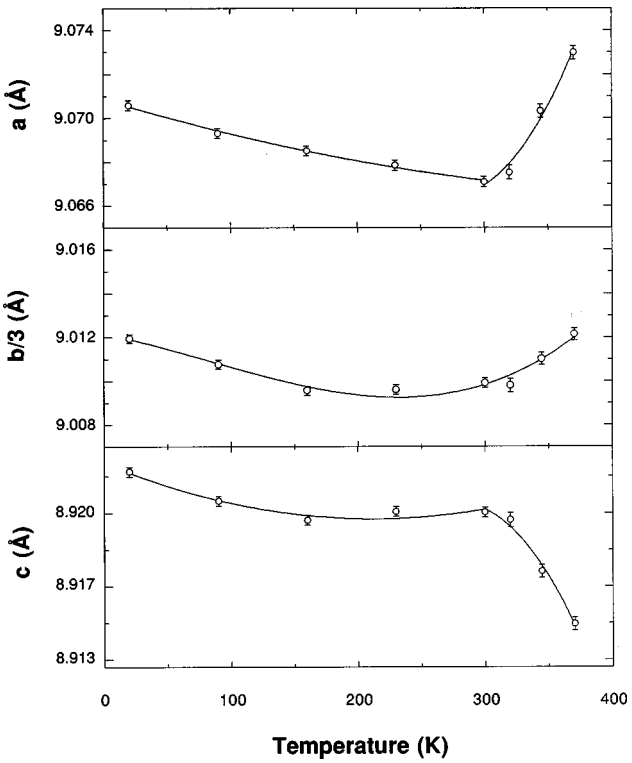

FIG. 11. Lattice parameters of orthorhombic γ-ZrW_2O_8 in the temperature range below the transition back to the cubic phase.

creases with temperature. Because c is the shortest lattice parameter, its pretransition decrease results in diverging orthorhombic lattice parameters just before the transition to the cubic phase. Thus, this pretransition behavior does not have the expected behavior for fluctuations towards the cubic α phase. There is apparently some other kind of structural instability that is then interrupted by the transition to the cubic α phase. We propose two possible explanations for this pretransition anomaly. First, it is possible that there are large fluctuations of the structure away from the metastable orthorhombic phase, but toward a larger-volume configuration different from the cubic α phase. The transition to the cubic α phase could occur before this intermediate phase forms in a coherent way. Second, it is possible that a phase transition to an intermediate phase does occur and we are not able to identify it from our diffraction data because of its complexity and similarity to the orthorhombic phase. The complexity of the orthorhombic phase structure is already near the limit of what can be refined using data from the Special Environment Powder Diffractometer. Further studies of this curious pretransition behavior will require better experimental resolution.

CONCLUSIONS

It is instructive to view the behavior of ZrW_2O_8 in terms of a conceptual free-energy picture that includes only the possible structural configurations for ZrW_2O_8. We conclude that (of the configurations that are kinetically allowed for this synthesis procedure) the cubic α phase is energetically favored at ambient pressure and room temperature. Upon increasing pressure above 0.21 GPa, as a result of changes in the topology of the energy surface resulting from the response of the cubic structure to applied pressure, the orthorhombic γ phase becomes the lowest energy phase that can be reached by an energetically allowed transition from the cubic phase. The transition to the orthorhombic phase is first order, meaning that there is an energy barrier between the cubic and orthorhombic minima, and involves a 5% volume reduction. The fact that the orthorhombic phase is retained upon the release of pressure shows that the energy minimum associated with this phase exists in the energy surface at ambient pressure. The energy barrier for transformation back to the energetically favored cubic phase is large enough that the transformation does not occur until the material is heated above 390 K.

The observation of a pressure-induced cubic-to-orthorhombic transition in ZrW_2O_8 is a manifestation of the thermodynamic principles that must apply to a material with negative thermal expansion. Maxwell's relation,

$$(\delta V/\delta T)_P = -(\delta S/\delta P)_T, \tag{1}$$

requires that the entropy S must increase with increasing pressure P for a material with negative thermal expansion. Thus, materials with negative thermal expansion will exhibit the unusual phenomena that pressure-induced phase transitions will lead to more complex structures (i.e., structures with more structural degrees of freedom) at higher pressure. ZrW_2O_8 provides an especially interesting example of this phenomena. The cubic-to-orthorhombic transition occurs at a remarkably low pressure of 0.21 GPa and involves a substantial increase in the number of structural degrees of freedom. Upon increasing the pressure further, the material becomes amorphous over the pressure range of 1.5 to 3.5 GPa.[17] Interestingly, the amorphous phase is also retained upon release of pressure. Although the structure of the amorphous phase has not yet been characterized, one might speculate that it involves random static inversions of W_2O_8 units, leading to a large number of possible configurations (consistent with the required increase in entropy), with many of the other features of the short-range structure remaining intact. However, the metastable amorphous phase does not transform back to the cubic phase at ambient pressure unless it is heated to quite high temperatures (923 K), suggesting that the structural rearrangements may be more extensive than those resulting from random inversions.

Landau and Lifshits[18] have derived an interesting relationship between the bulk thermal expansion of a material and the correlation between fluctuations of entropy and volume:

$$\langle \Delta S \Delta V \rangle = kT(\delta V/\delta T)_P, \tag{2}$$

where ΔS and ΔV are the correlated entropy and volume fluctuations in a local region of the body and the brackets $\langle\ \rangle$ indicate an average over all such local regions. From this equation, one learns that the entropy and volume fluctuations must be anticorrelated (on average) in a material with negative thermal expansion; i.e., in a localized region of the body, a fluctuation that increases the entropy will decrease the volume. The proposed mechanism for negative thermal expansion in ZrW_2O_8, based on rigid unit modes that pull the entire structure inward as the amplitudes of vibration increase, is consistent with this equation.

The thermally excited inversion of W_2O_8 units could also provide a mechanism for negative thermal expansion satisfying Eq. (2). The observation of a 5% volume reduction when 1/3 of the W_2O_8 units are inverted in the cubic-to-orthorhombic transition suggests that fluctuations that produce an inversion could locally reduce the volume. It is not clear whether such fluctuations actually contribute a significant amount to the negative thermal expansion of ZrW_2O_8. Because the number of thermally excited inversions is likely to be small except for temperatures just below the α-to-β transition, one might speculate that this contribution is only significant in that temperature range. Interestingly, the negative thermal expansion exhibits its largest magnitude in the α phase just below the transition to the β phase,[1,2] where a contribution from thermally excited inversions could add to that of the rigid unit modes.

The concepts discussed above provide a general framework for understanding negative thermal expansion in complex structures like ZrW_2O_8 and can suggest what kinds of additional materials should be investigated for such behavior. The complexity of the energy surface for ZrW_2O_8 is, in a qualitative sense, a result of unusual features of the structure, such as the significant differences between the two inequivalent WO_4 tetrahedra, the large degree of polyhedral distortion, and the one-coordinated oxygen atom. Negative thermal expansion over a large temperature range has already been discovered in other complex open-framework structures[3,4] and more new compounds are likely to follow. Understanding the response of such structures to pressure is important for several reasons. First, structural measurements vs pressure can provide a useful view of the flexibility of the structure, showing what structural degrees of freedom may be important in the negative thermal expansion. Second, as in the case of ZrW_2O_8, pressure may produce a transformation to a closely related phase whose thermal expansion properties can be compared with those of the ambient-pressure phase. Third, understanding the response to pressure is directly relevant to the behavior of the negative-thermal-expansion material in a composite, where grain-interaction stresses can produce large local pressures.

ACKNOWLEDGMENTS

The work at Argonne National Laboratory was supported by the U.S. Department of Energy, Division of Basic Energy Sciences-Materials Sciences, under Contract No. W-31-109-ENG-38 (J.D.J., S.S., S.T., Z.H.) and by the National Science Foundation, Office of Science and Technology Centers, Grant No. DMR-91-20000 (D.N.A.). The work at the Oregon State University was supported by the National Science Foundation Grant No. DMR-9308530 and the Oregon Metals Initiative. J.S.O.E. would like to thank the Royal Commission for the Exhibition of 1851 for financial support.

*Present address: Manuel Lujan Neutron Scattering Center, MS H805, Los Alamos National Laboratory, Los Alamos, NM 87545.
†Address after September 1998: Department of Chemistry, University of Durham, Science Laboratories, South Road, Durham DH1 3LE, UK.

[1] T. A. Mary, J. S. O. Evans, T. Vogt, and A. W. Sleight, Science **272**, 90 (1996).
[2] J. S. O. Evans, T. A. Mary, T. Vogt, M. A. Subramanian, and A. W. Sleight, Chem. Mater. **8**, 2809 (1996).
[3] J. S. O. Evans, T. A. Mary, and A. W. Sleight, J. Solid State Chem. **133**, 580 (1997).
[4] J. S. O. Evans, T. A. Mary, and A. W. Sleight, J. Solid State Chem. **137**, 148 (1998).
[5] V. Korthuis, N. Khosrovani, A. W. Sleight, N. Roberts, R. Dupree, and W. W. Warren, Chem. Mater. **7**, 412 (1995).
[6] T. A. Mary, V. Korthuis, N. Khosrovani, and A. W. Sleight, *Low Expansion Materials* (American Ceramic Society, Westerville, OH, 1995), Vol. 32, pp. 81.
[7] R. Roy, D. K. Agrawal, and H. A. McKinstry, Annu. Rev. Mater. Sci. **19**, 59 (1989).
[8] A. K. A. Pryde, K. D. Hammonds, M. T. Dove, V. Heine, J. D. Gale, and M. C. Warren, J. Phys.: Condens. Matter **8**, 1 (1996).
[9] A. K. A. Pryde, Phase Transit. **61**, 141 (1997).
[10] J. S. O. Evans, Z. Hu, J. D. Jorgensen, D. N. Argyriou, S. Short, and A. W. Sleight, Science **275**, 61 (1997).
[11] J. D. Jorgensen, J. J. Faber, J. M. Carpenter, R. K. Crawford, J. R. Haumann, R. L. Hittermann, R. Kleb, G. E. Ostrowski, F. J. Rotella, and T. G. Worton, J. Appl. Crystallogr. **22**, 321 (1989).
[12] J. D. Jorgensen, S. Pei, P. Lightfoot, D. G. Hinks, B. W. Veal, B. Dabrowski, A. P. Paulikas, R. Kleb, and I. D. Brown, Physica C **171**, 93 (1990).
[13] A. C. Larson and R. B. Von Dreele, General Structure Analysis System, Los Alamos Internal Report No. 86-748, 1985–1990 (unpublished).
[14] Using the program DLS-76: Ch. Baerlocher, A. Hepp, W. M. Meier, Institute of Crystallography, 7 ETH, Switzerland, 1977.
[15] R. M. Hazen and C. T. Prewitt, Am. Mineral. **62**, 309 (1977).
[16] D. Altermatt and I. D. Brown, Acta Crystallogr., Sect. B: Struct. Sci. **41**, 240 (1985).
[17] C. A. Perottoni and J. A. H. da Jornada, Science **280**, 886 (1998).
[18] L. D. Landau and E. M. Lifshits, *Statistical Physics* (Pergamon, New York, 1958), p. 356.